JACS
JOURNAL OF THE AMERICAN CHEMICAL SOCIETY

ARTICLE

pubs.acs.org/JACS

Cooperative Hybridization of Oligonucleotides

David Yu Zhang*

California Institute of Technology, Pasadena, California 91125, United States

Supporting Information

ABSTRACT:

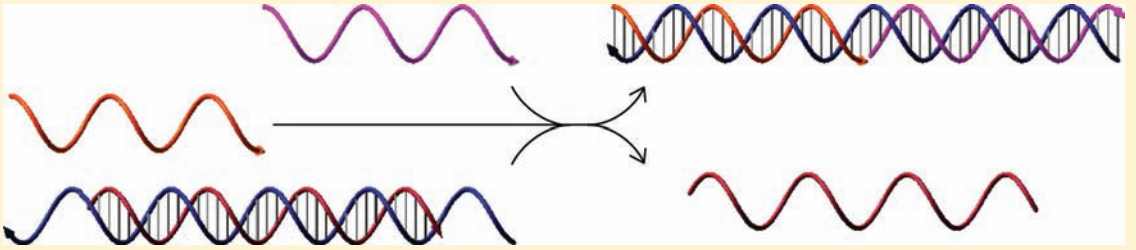

Nucleic acids have been demonstrated to be versatile nanoscale engineering materials with the construction of dynamic DNA structures, motors, and circuits. These constructions generally rely on the clever use and integration of relatively few reaction mechanisms and design primitives. Here, cooperative hybridization is introduced as a mechanism in which two oligonucleotides of independent sequence can stoichiometrically, simultaneously, and cooperatively hybridize to a DNA complex. Cooperative hybridization is rigorously characterized and modeled and is shown to implement digital concentration comparison with amplification, as well as digital Boolean logic. These designs, based on cooperative hybridization, excel in being robust to impurities and not requiring oligonucleotide purification.

INTRODUCTION

The precise temporal and spatial control of molecules is a fundamental goal of both synthetic biology and nanotechnology and is essential for building reliable nanoscale structures and devices. Nucleic acids, by virtue of their well-understood hybridization thermodynamics and kinetics,[1] exponential information content and 0.4 nm addressability,[2] and economy of synthesis and preparation,[3] have emerged as a leading material for nanoscale engineering.[4−9] Furthermore, the biological relevance of nucleic acids[10,11] and the ease of coupling nucleic acids to other materials, such as proteins[12] and carbon nanotubes,[13] facilitate the use of nucleic acids both as synthetic biomaterials and as scaffolds for other nanotechnological applications.

Although the first generation of DNA nanotechnology research has focused on the self-assembly of static DNA nanostructures,[14−18] recent works in the field have also expanded into the realm of constructing dynamic nucleic acid devices, in which nucleic acid nanostructures conditionally and programmably reconfigure in solution.[8,9] Examples include cascaded logical and amplification circuits,[19−27] DNA origami boxes that close and open,[28] molecular walkers that traverse predefined landscapes,[29−32] controlled rotating DNA frameworks,[33−35] and chain reaction DNA motors and dendrimers.[36−38]

While some of these constructions relied on functional nucleic acid molecules with innate catalytic activity (known as ribozymes and deoxyribozymes),[19−22,29,30] many others were constructed using purely rational design approaches, based on the well-characterized thermodynamic[1,39] and kinetic[40,41] properties of DNA hybridization, branch migration, and dissociation processes. The latter group generally relies the clever and repeated use of a simple but reliable mechanism, known as toehold-mediated strand displacement, in which short, single-stranded domains on different DNA molecules hybridize to colocalize the molecules, enabling subsequent branch migration.[9,33] To further expand the scope of functions achievable with dynamic DNA nanotechnology, it is necessary to develop other molecular mechanisms that afford functionality that toehold-mediated strand displacement cannot achieve.

Here, a generalized method for implementing cooperative hybridization is presented, in which two oligonucleotides (targets) of independent sequence simultaneously and cooperatively bind to a designed two-stranded complex. The complex allows the two targets to stoichiometrically react and colocalize with each other, much in the same way that two complementary oligonucleotides hybridize to each other.

In contrast to toehold-mediated strand displacement reaction networks, which primarily rely on sequential hybridization and branch migration events, cooperative hybridization enables parallel hybridization and branch migration events to occur. In addition to enabling networks such as amplified digital detection of over- and under-expression relative to a threshold, cooperative hybridization also offers the practical advantage of being robust to synthesis impurities and a background of unrelated nucleic acids and thus is likely to be a useful tool for engineering dynamic DNA nanotechnological devices.

Received: October 18, 2010
Published: December 17, 2010

dx.doi.org/10.1021/ja109089q | J. Am. Chem. Soc. 2011, 133, 1077–1086

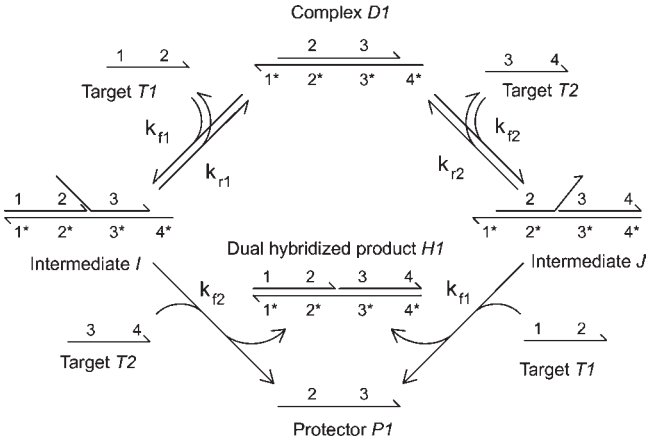

Figure 1. Cooperative hybridization mechanism. Two nucleic acid molecules of interest, *T*1 and *T*2, cooperatively hybridize to two-stranded complex *D*1 (composed of upper strand *P*1 and lower strand *L*1). *T*1 and *T*2 individually bind to *D*1 in a reversible manner, but their simultaneous binding releases protector strand *P*1 and dual-hybridized product *H*1, rendering the reaction irreversible. DNA strands are represented as directional lines, with the hook denoting the 3′ end. Each strand is subdivided into domains, continuous nucleotides that act as a unit in hybridization, branch migration, or dissociation. Domains are represented by numbers, and starred domains denote complements of the unstarred domains (e.g., 2* is complementary to 2). The $T1+D1 \rightarrow I$ and $T1+J \rightarrow P1+H1$ reactions are assumed to have identical rate constants because these reactions are initiated by identical single-stranded toeholds, and similarly for the $T2+D1 \rightarrow J$ and $T2+I \rightarrow P1+H1$ reactions. Previous research has shown that the rate constant of strand displacement reactions are primarily determined by the standard free energy of toehold hybridization.[40]

COOPERATIVE HYBRIDIZATION MECHANISM

The cooperative hybridization mechanism is shown in Figure 1. Two target strands, *T*1 and *T*2, hybridize simultaneously to two-stranded complex *D*1 only when both are present. There are two parallel pathways for this reaction. In one, *T*1 first binds to *D*1 form intermediate *I*, which then reacts with *T*2 to form *H*1 and release product strand *P*1. In the other pathway, *T*2 binds first to *D*1 to form intermediate *J*. Individually, the hybridization of *T*1 or *T*2 to *D*1 is reversible and thermodynamically unfavorable; the release of product *P*1 upon the simultaneous hybridization of *T*1 and *T*2 facilitates the net reaction.

The cooperative hybridization mechanism can be expressed as the following reactions:

$$T1 + D1 \rightleftharpoons I$$

$$T2 + D1 \rightleftharpoons J$$

$$T2 + I \rightarrow P1 + H1$$

$$T1 + J \rightarrow P1 + H1$$

The net reaction of the system is thus

$$T1 + T2 + D1 \rightarrow P1 + H1$$

There are three prominent features of this reaction. First, the net reaction possesses different numbers of reactants and products, making the equilibrium distribution of the reactants and products concentration dependent. At low concentrations, entropy is a larger factor, and reactants will exist at higher concentration at equilibrium, while the opposite is true at high concentrations. At operational conditions, the products are designed to be predominant.

Second, at operational concentrations where the products are favored, the equilibrium concentration of *P*1 will be roughly the minimum of the initial concentrations of *T*1, *T*2, and *D*1. As *P*1 is a strand with a different sequence than both *T*1 and *T*2, it can potentially participate in downstream reactions that *T*1 and *T*2 cannot. Thus, the cooperative hybridization mechanism not only allows the two target oligonucleotides to be colocalized but also releases a third oligonucleotide to signal the completion of the cooperative hybridization reaction.

Third, because the individual reaction of *T*1 or *T*2 with *D*1 is thermodynamically unfavorable, at operational concentrations very little of *T*1 or *T*2 is sequestered in *I* or *J* if only one of *T*1 or *T*2 is present. The equilibrium concentration of free *T*1 or *T*2 in this case would be near the total concentration of *T*1 or *T*2. These properties of the cooperative hybridization process allow a variety of useful dynamic nucleic acid devices and circuits.

MATERIALS AND METHODS

DNA Sequences and Design. The conceptual design of the system, such as the domain lengths and relative binding strengths, was based on the expected operational concentration and the desired binding fraction of individual targets in the absence of the second target. In particular, domains 1 and 4 were designed so that, individually, their hybridization energies were insufficient to overcome the entropic loss of colocalizing one additional molecule of DNA, but collectively, they do drive the reaction forward. These considerations are discussed in mathematical detail in Supporting Information, S1.

The sequences were designed subsequently using domain-based sequence design software.[42] The domains (shown in Table 1) possess minimal secondary structure and crosstalk (binding between unrelated domains): NUPACK[39] (http://www.nupack.org/) calculates there to be no more than four paired bases between any pair of strands at 25 °C, even at 1 μM concentration. Furthermore, the minimum free energy states of every individual strand was completely unstructured ($\Delta G^\circ = 0$). Thus, the domains we use can be approximated as structure-free. Substantial secondary structure is known to slow down branch migration and interfere with hybridization.[43]

Standard Free Energy Calculation. The standard free energies of complexes are needed in order to calculate the standard free energy of reactions, which in turn can be used to generate equilibrium and rate constants. NUPACK[39] was used to calculate the standard free energies of DNA complexes. NUPACK uses a number of different parameters in its calculations; the values used are detailed and justified below.

Temperature was set to 25 °C, as that was the temperature at which experiments were performed. Salt concentration was set to 0.05 M Na^+ and 0.0115 M Mg^{2+}. In actuality, the experimental concentration of Na^+ is 0.002 M, but 0.05 M Na^+ was the lowest NUPACK allowed. However, since Mg^{2+} acts as the main counterion, it is likely that this difference does not significantly change the standard free energies.

The "dangles" parameter was set to ALL, so that dangles energies are incorporated for all bases flanking duplexes, regardless of whether it is paired. This is necessary because, by default, NUPACK does not incorporate the thermodynamics of coaxial stacks (such as at the nick in *I*, *J*, and *H*1). The reason NUPACK does not by default include coaxial stacking thermodynamics is that they are still not well-understood: Pyshnyi et al.[44] report that the energetics of coaxial stacking near a nick depends significantly on the nearest neighbors (bases one away from the nick). Setting dangles = ALL allows partial compensation of the energetics at the nicks.

The standard free energies of complexes determine the standard free energies of reactions, which in turn can be used to calculate the equilibrium constant of the reaction via $\Delta G^\circ = -RT \ln(K_{eq})$. For a reaction with different numbers of reactants and products, K_{eq} is not unitless, and

Table 1. Domain and Strand Sequences[a]

domain	sequence	length (nt)
1	5′-CATCACTA-3′	8
2 = 2a:2b:2c	5′-CTATCATCACACATCTAT-3′	18
2a	5′-CTATCAT-3′	7
2b	5′-CACACAT-3′	7
2c	5′-CTAT-3′	4
3 = 3a:3b	5′-ACAACCACTTACTTCTTC-3′	18
3a	5′-ACAACCACTTACTT-3′	14
3b	3′-CTTC-3′	4
4	5′-ATCTATCC-3′	8
5	5′-CTATCAT-3′	7
6	5′-CACACAT-3′	7
7	5′-CTATACAACCACTTACTT-3′	18
8	5′-CTTC-3′	4
9	5′-GCCATCAGAACTTAACCT-3′	18
10	5′-AACTC-3′	5
11	5′-CTTTCCTACA-3′	10
12a	5′-CCTACGTCTC-3′	10
12b	5′-CAACTAA-3′	7
12c	5′-CTTACGG-3′	7
13	5′-CCCTC-3′	5

strand	domain composition	length (nt)
*T*1	1 2	26
*T*2	3 4	26
*P*1	2 3	36
*L*1	4* 3* 2* 1*	52
F	2c 3a	18
RL	3a* 2c* 2b*	25
*T*3	5 6 7 8	36
*T*4	9 10 ROX	23
*P*2	7 9	36
*L*2	RQ 10* 9* 7* 6*	48

[a] The sequences of the starred complement domains are determined by the corresponding unstarred domains. For example, the 10 domain has sequence 5′-AACTC-3′, so 10* has sequence 5′-GAGTT-3′. Strands are shown as concatenations of domains, listed from 5′ to 3′ end.

its value will depend on its unit. Thus, the ΔG° of a reaction may depend on the units used for expressing K_{eq}. For example, K_{eq} = 1 M is identical to saying K_{eq} = 1000 mM, but the former yields ΔG° = 0 kcal/mol, while the latter yields $\Delta G^\circ = -4.1$ kcal/mol at 25 °C.

NUPACK reports the ΔG° values of complexes based on the equilibrium constant of the complex's formation, calculated in mole fraction. Because the concentration of all nucleic acid molecules is negligible compared to that of water ((1000 g/L)/(18 g/mol) = 55 M), the molarity of the oligonucleotides is roughly 1/55th that of their mole fractions. To convert the NUPACK reported ΔG° into one that yields K_{eq} expressed in molar, we add a corrective $(n-1)RT\ln(55)$ term, where n denotes the number of strands the DNA molecule possesses (i.e., +2.38 kcal/mol for every strand in excess of 1).

Intermediates *I* and *J* represent the three-stranded complexes on which branch migration is possible (domain 2 for *I* and domain 3 for *J*). Consequently, *I* and *J* each correspond to 19 isoenergetic branch migration states (I_0 through I_{18} and J_0 through J_{18}, respectively). Each

Table 2. Composition and Standard Free Energies of Complexes Shown in Figures 1 and 2[a]

complex	strand composition	calcd ΔG° (kcal/mol)
*D*1	*P*1, *L*1	−49.27 + 2.38 = −46.9
I	*P*1, *L*1, *T*1	−62.15 + 2(2.38) − 1.75 = −59.1
J	*P*1, *L*1, *T*2	−61.51 + 2(2.38) − 1.75 = −58.5
*H*1	*L*1, *T*1, *T*2	−70.69 + 2(2.38) = −65.9

[a] The standard free energies of these complexes were calculated using NUPACK,[39] using the parameters 25 °C, 0.05 M Na^+, 0.0115 M Mg^{2+}, dangles = ALL. The standard free energies of all individual strands were 0 kcal/mol (completely unstructured). Because NUPACK yields ΔG° values that were calculated for mole fraction rather than molar, a corrective $RT\ln([H_2O])$ = +2.38 kcal/mol term must be added for every strand in excess of 1. The intermediate states *I* and *J* each correspond to 19 isoenergetic branch migration states; the $-RT\ln(19)$ = −1.75 kcal/mol term corrects for this state multiplicity.

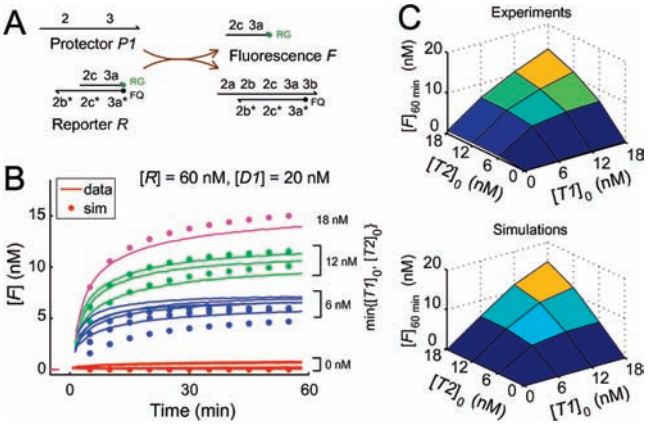

Figure 2. Characterizing and modeling cooperative hybridization. (A) The kinetics of the cooperative hybridization reaction are assayed through the use of a fluorescence reporter complex *R* (comprised of *F* and *RL*). *P*1 reacts stoichiometrically with *R* to release fluorophore-labeled strand *F*. RG denotes Rhodamine Green, and FQ denotes the Iowa Black Fluorescence Quencher. (B) Kinetics of cooperative hybridization. *R* and *D*1 were present in solution initially, and various quantities of *T*1 and *T*2 were introduced at time $t \approx 0$. Because *D*1 is in excess of both *T*1 and *T*2, both the kinetics and the final equilibrium fluorescence value depend on the minimum of the concentrations of *T*1 and *T*2. The dotted lines show simulation results using experimentally measured rate constants (see Table 3, Supporting Information, S3 and Figure S1). (C) Summary of experimental and simulations results, with fluorescence plotted against the concentrations of *T*1 and *T*2. This figure shows that the release of *P*1 (and subsequently *F*) is contingent upon the simultaneous presence of *T*1 and *T*2.

of these states has a ΔG° calculated by NUPACK to satisfy the equilibrium constant in one of the following reactions:

$$T1 + D1 \rightleftharpoons I_0 \rightleftharpoons I_1 \cdots I_{17} \rightleftharpoons I_{18}$$

$$T2 + D1 \rightleftharpoons J_0 \rightleftharpoons J_1 \cdots J_{17} \rightleftharpoons J_{18}$$

The standard free energies of the amalgamate states *I* and *J* are defined so as to preserve the equilibrium concentrations of *D*1 and *T*1 or *T*2. To do so, $-RT\ln(19) = -1.75$ kcal/mol is added to the ΔG° of a single I_0 or J_0 state, respectively, to derive the ΔG° of *I* or *J*.

Table 2 shows the calculated free energies of the complexes.

Annealing. All annealing processes were performed with an Eppendorf Mastercycler Gradient thermocycler. The samples were brought down from 95 to 20 °C at a constant rate over the course of 75 min.

dx.doi.org/10.1021/ja109089q | J. Am. Chem. Soc. 2011, 133, 1077–1086

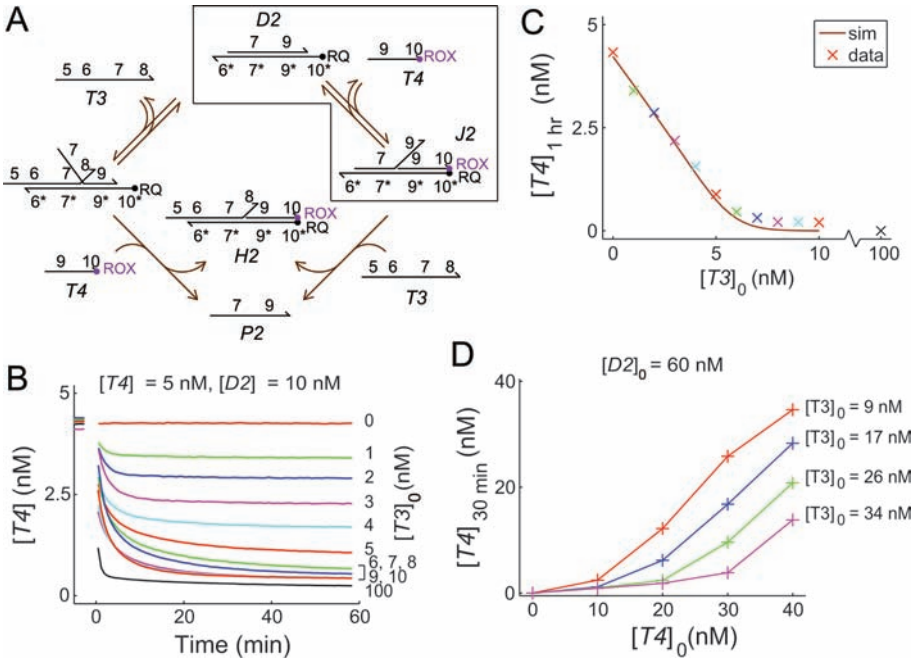

Figure 3. Demonstration of cooperativity. (A) *T*3 and *T*4 cooperatively hybridize to *D*2. *T*4 is fluorophore-labeled, and the bottom strand of *D*2 is quencher-labeled. When *T*4 is hybridized to *D*2, the fluorophore is colocalized to the quencher and fluorescence decreases. In the absence of *T*3, *T*4 should not significantly bind to *D*2 at the operational conditions, so fluorescence should be high. The box shows the species present before *T*3 is added. (B) Experimental results support the proposed mechanism. *D*2 and *T*4 are initially present, and fluorescence is similar to that of *T*4 alone. As various amounts of *T*3 are introduced into the reaction at $t \approx 0$, the fluorescence decreases. (C) Summary of the results in (B). Fluorescence after 1 h follows a kinked line, with the kink roughly at $[T3] = 5$ nM; errors in the concentration of the stock solutions of *T*3 and *T*4 likely contribute to the kink deviating from 5 nM. In fact, the cooperative hybridization mechanism can be used as a method of quantitating nucleic acid concentrations given a known standard of independent sequence (see also Supporting Information, S4 and Figure S3). Simulation traces shows the predicted results according to our model, fitting the *T*3 concentration to be 14% lower than as measured by absorbance. (D) The equilibrium concentration of free *T*4 (which is roughly linear to fluorescence) is the difference between the initial concentrations of *T*4 and *T*3. Data displayed shows the fluorescence after 30 min, as a function of *T*3 and *T*4 concentration. Fluorescence appears to be roughly linear in the concentration excess of *T*4 over *T*3. This figure shows that the individual binding of *T*3 or *T*4 to *D*2 is reversible and not favorable at equilibrium, and that the hybridization mechanism is cooperative as designed.

Complex Purification. DNA oligonucleotides used in this study were purchased from Integrated DNA Technologies (IDT). Where applicable, fluorophores were attached by IDT as well. Concentrations were determined from the measured absorbance at 260 nm using an Eppendorf Biophotometer and calculated extinction coefficients.[45,46]

Complex *D*1 used in Figure 2 was purified by non-denaturing (ND) polyacrylamide gel electrophoresis (PAGE) to ensure proper stoichiometry as follows: The *P*1 and *L*1 strands were prepared with nominally correct stoichiometry at 20 μM and annealed. The samples were then run on 12% ND PAGE at 180 V for 6 h.

The acrylamide (19:1 acrylamide:bis) was diluted from 40% acrylamide stock (Ambion). ND loading dye containing xylene cyanol FF in 50% glycerol was added to all samples, achieving a final gycerol concentration of 10% by volume. Gels were run at 25 °C using a Novex chamber with an external temperature bath.

The proper *D*1 band was cut out and eluted in 2 mL of TE/Mg^{2+} buffer for 2 days. Purified complexes were quantitated by 260 nm absorbance measurement and calculated extinction coefficients. Yield was approximately 50%.

Notably, only the complex *D*1 used for experiments in Figure 2 was purified; the *D*2 used in Figure 3 and the *D*1 used in Figures 4−6 were not purified.

Buffer Conditions. DNA oligonucleotides were stored in TE buffer (10 mM Tris·HCl pH-balanced to 8.0, with 1 mM EDTA·Na_2, purchased as 100x stock from Sigma-Aldrich) at 4 °C. Directly preceding experiments, TE buffer with 62.5 mM $MgCl_2$ was added at a 1:4 ratio to the sample, achieving a final $MgCl_2$ concentration of 12.5 mM (of which 1 mM is bound to EDTA). This buffer is henceforth known as "TE/Mg^{2+}" buffer. All experiments and purifications were performed at 25 ± 0.5 °C, with temperature controlled using an external temperature bath.

Spectrofluorimetry Studies. Spectrofluorimetry studies were done using a SPEX Fluorolog-3 (Horiba) with 1.6 mL 119-004F synthetic quartz cells (Hellma). For the experiments shown in Figures 3, 5D, and 6, excitations were at 588 nm, while emissions were at 602 nm (optimal signal for ROX fluorophore). For the experiments shown in Figures 2, 4, and 5B, excitations were at 510 nm, while emissions were at 531 nm (optimal signal for Rhodamine Green fluorophore). In all spectrofluorimetry experiments, the total reaction volume was 1.5 mL. For Figures 3B,C, 5E, 6, and S2A−C, 4 nm band-pass slits were used for both excitation and emission monochromators. For all other experiments, 2 nm slits were used. In all experiments, data points were collected with an integration time of 10 s for every 60 s time point.

Prior to each experiment, all cuvettes were cleaned thoroughly: each cuvette was washed 15 times in distilled water, once in 70% ethanol, another five times in distilled water, and finally once more in 70% ethanol.

For the slit size, concentrations, and times chosen, no measurable photobleaching was observed. All experimental results were within the linear regime of the spectrofluorimeter detector, according to the specification sheets provided by the manufacturer.

Fluorescence Normalization. Fluorescence is normalized so that 1 normalized unit (n.u.) of fluorescence corresponds to 1 nM of an unquenched fluorophore-labeled strand (*F* in Figures 2 and 5B, *T*4 in Figures 3, 5D, and 6, and *F*2 in Figure 4). This normalization is based on the fluorescence levels of annealed samples: A negative control with [*R*]

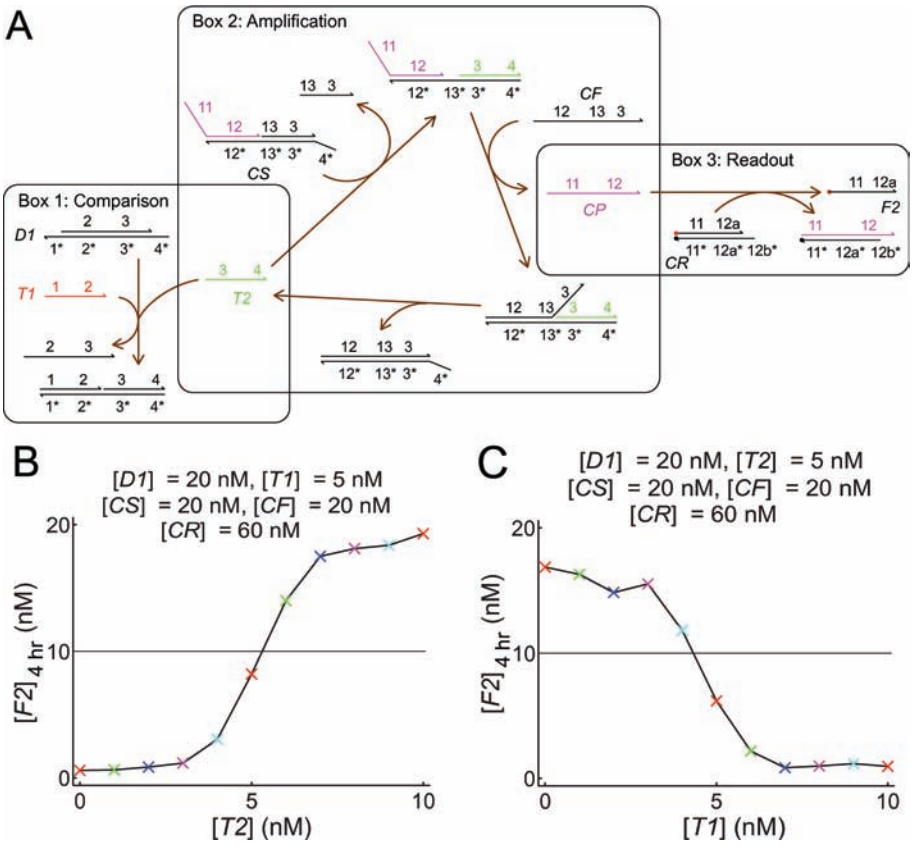

Figure 4. Application: amplified digital detection of over- and under-expression relative to a threshold. (A) Schematic. The detection circuit is divided into three modular components, shown as boxes. For over-expression detection, *T*1 serves as the threshold and is present at known concentration. If the amount of *T*2 exceeds that of *T*1, then the excess *T*2 catalyzes the release of *CP* from *CS*, which in turn reacts stoichiometrically with fluorescent reporter *CR* to release fluorophore-labeled strand *F*2 (see also ref 25). For under-expression detection, *T*2 serves as the threshold with known concentration and will trigger the catalytic pathway unless excess *T*1 is added. (B) Over-expression detection. Fluorescence increases as $[T2]_0$ exceeds the threshold set by $[T1]_0$. *T*2 is pre-reacted with *D*1 and *T*1 for 15 min, and then *CF*, *CS*, and *CR* are added to solution to begin the reaction. Maximum fluorescence (gain) is determined by [*CF*], [*CS*], and [*CR*], the concentrations of the catalytic substrate and reporter species. (C) Under-expression detection. Fluorescence decreases as $[T1]_0$ exceeds the threshold set by $[T2]_0$.

= 30 nM yielded the fluorescence of the quenched *F* strand (Rhodamine Green), and a positive control with [*R*] = 30 nM and [*P*1] = 10 nM yielded the fluorescence of the unquenched *F* strand. Similarly, a negative control with [*T*4] = 5 nM and [*L*2] = 10 nM yielded the fluorescence of the quenched *T*4 strand (ROX), and a positive control with [*T*4] = 5 nM yielded the fluorescence of the unquenched *T*4 strand.

Day-to-day and sample-to-sample variations in fluorescence are estimated to be less than 5%.

Ordinary Differential Equation (ODE) Simulations. Reaction simulations were run in Matlab using the "stiff" ode23s solver because of the difference in time scales of bimolecular and unimolecular reactions. The relative tolerance of the solver was set to 10^{-4}, and the absolute tolerance of the solver was set to 10^{-30} M. Supporting Information, S2 shows sample code for simulating the system shown in Figure 2.

Parameter Fitting. Rate constants were fitted to experimental data using the "fminunc" function in Matlab to minimize the error between experimental data and the reaction model. The error between the data and the simulation is calculated as

$$\text{Error} = \sum_{t,\,\text{traces}} (F_d(t) - F_m(t))^2$$

where $F_d(t)$ is the fluorescence value of the data at time *t*, and $F_m(t)$ is the fluorescence value predicted by the ODE model at time *t*. Sample code for fitting the rate constants is shown in Supporting Information, S2.

The confidence intervals on the values of the rate constants were generated as the values of the rate constant at which the error score is double that of the minimum. All other rate constants were kept constant at their best-fit values when generating the confidence interval on each rate constant.

RESULTS

Characterizing Cooperative Hybridization. To demonstrate that the cooperative hybridization mechanism functions as intended, two different properties must be independently verified: first that *T*1 and *T*2 when simultaneously present can cooperatively hybridize to *D*1, and second that *T*1 in the absence of *T*2 or *T*2 in the absence of *T*1 is insufficient to stably bind *D*1.

Figure 2 shows the kinetic behavior of the cooperative hybridization system through the use of a fluorescent reporter complex *R* that reacts stoichiometrically with *P*1. The release of *P*1 and the subsequent fluorescence increase is seen to vary linearly with the minimum of the initial concentrations of *T*1 and *T*2, supporting the proposed mechanism.

Also shown in Figure 2B,C are simulation results, using individually measured rate constants (see Supporting Information, S3 and Figure S1). The reactions simulated and their relevant rate constants are summarized in Table 3. The agreement between

dx.doi.org/10.1021/ja109089q | *J. Am. Chem. Soc.* 2011, 133, 1077–1086

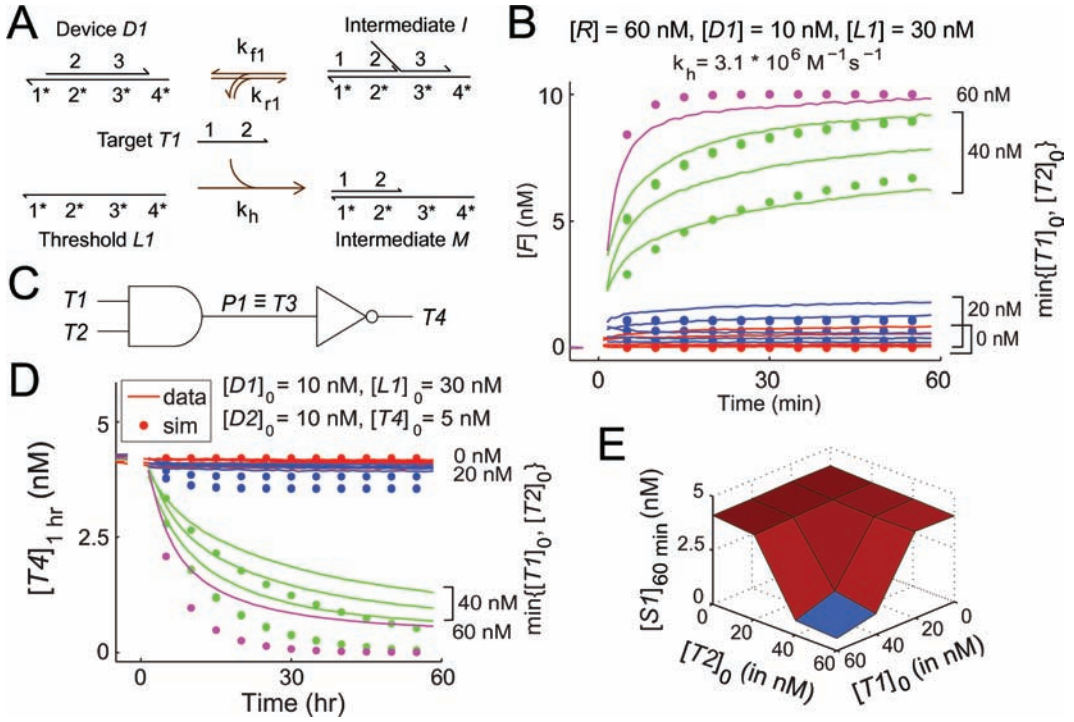

Figure 5. Application: cascaded nucleic acid logic. (A) Thresholding using the bottom strand *L*1 of *D*1. Targets *T*1 and *T*2 preferentially bind *L*1 over *D*1 because *L*1 offers a longer single-stranded toehold for initiating hybridization and because individual hybridization is irreversible. (B) Experimental and simulation results of cooperative hybridization with a threshold. The fluorescence increases quickly when the concentrations of both targets *T*1 and *T*2 exceed that of the threshold *L*1. (C) The *P*1 species from Figures 1 and 2 was designed to be identical in sequence to *T*3 in Figure 3. Consequently, the logical AND and the logical NOT gates can be directly cascaded to form a network exhibiting NAND logic. (D) Experimental data and simulations on the logical NAND cascaded network. *D*1, *L*1, *D*2, and *T*4 were present in solution initially, *T*1 and *T*2 were added at time $t \approx 0$. No new parameters were fit to the data shown in this figure; rate constants simulated were fitted in previous figures. (E) 3D summary of the experimental results in part (D).

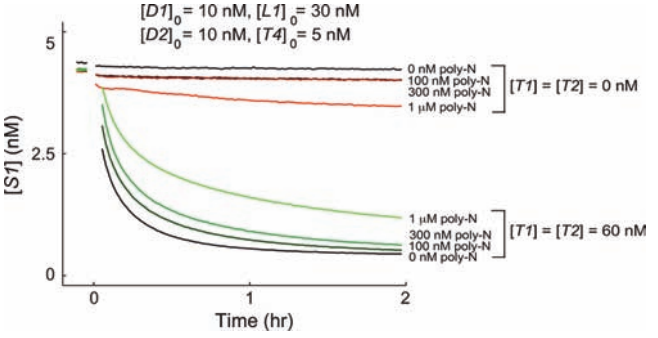

Figure 6. Robustness to background molecules. Various amounts of poly-N mix (50 nt oligonucleotides with a random distribution of G, C, A, and T bases at every position) were added the NAND reaction network. *D*1, *L*1, *D*2, and *T*4 were present in solution initially; *T*1, *T*2, and poly-N were added at time $t \approx 0$.

ODE simulations and experimental data further supports that the cooperative hybridization mechanism functions as designed: the consumption of *T*1, the consumption of *T*2, and the production of *P*1 are all simultaneous and stoichiometric with respect to each other. The small quantitative differences between simulations and experiments are likely due to oligonucleotide impurities (see Supporting Information, S6 and Figure S5) and undocumented side reactions (such as $T2 + R \rightarrow F$).

Figure 3 demonstrates that the two DNA oligonucleotide targets do not unilaterally bind irreversibly to the two-stranded complex. Here, different sequences are used, with *T*3 and *T*4 cooperatively hybridizing to complex *D*2. *T*4 is labeled with the ROX fluorophore, and the bottom strand *L*2 of the *D*2 complex is labeled with the Iowa Black Red Quencher. Thus, when *T*4 is hybridized to *D*2, either temporarily or permanently, the observed fluorescence is decreased. This allows a direct assay of the instantaneous concentration of free *T*4.

The other oligonucleotide target *T*3 possesses both 5′ and 3′ overhangs that serve no function for the cooperative hybridization mechanism. The existence of these overhangs demonstrates that the cooperative hybridization mechanism can be used to target a subsequence of a longer nucleic acid, such as an mRNA.

Figure 3B shows the results of this system. The fluorescence of solution in the absence of *T*3 is between 4 and 4.5 nM, while $[T4]_0 = 5$ nM. A small fraction of the *T*4 is associated to *D*2 at equilibrium. When an amount of *T*3 is added to the system, the fluorescence (concentration of free *T*4) re-equilibrates, consistent with our understanding of the cooperative hybridization mechanism.

The stoichiometric consumption of the two single-stranded reactants in cooperative hybridization can be interpreted as analog subtraction. If initially $[T4]_0 > [T3]_0$, then the equilibrium concentration of free *T*4 will be $[T4]_\infty \approx [T4]_0 - [T3]_0$. This property can be used to compare the concentrations of oligonucleotides of known sequences. For example, *T*4 can act as a well-characterized standard, and a different *D*2 complex can be constructed for each nucleic acid molecule *T*3 of interest. In a solution of a known quantity of *T*4 and an excess of *D*2, the concentration of *T*3 can be inferred from the equilibrium fluorescence (see Supporting Information, S4 and Figure S3). Because the same standard *T*4 can be used to quantitate a variety of

dx.doi.org/10.1021/ja109089q | *J. Am. Chem. Soc.* 2011, 133, 1077–1086

Table 3. Reaction Kinetics and Thermodynamics

Reactions and Rate Constants Simulated in Figure 2B,C[a]	
$T1 + D1 \underset{k_{r1}}{\overset{k_{f1}}{\rightleftharpoons}} I$	$k_{f1} = (2.1 \pm 0.7) \times 10^6\ M^{-1}\ s^{-1}$
$T2 + D1 \underset{k_{r2}}{\overset{k_{f2}}{\rightleftharpoons}} J$	$k_{f2} = (1.4 \pm 0.2) \times 10^6\ M^{-1}\ s^{-1}$
$T2 + I \xrightarrow{k_{r2}} P1 + H1$	$k_{r1} = 0.54 \pm 0.42\ s^{-1}$
$T1 + J \xrightarrow{k_{r1}} P1 + H1$	$k_{r2} = 0.39 \pm 0.27\ s^{-1}$
$P1 + R \xrightarrow{k_{rep}} F + Fw$	$k_{rep} = (1.3 \pm 0.5) \times 10^7\ M^{-1}\ s^{-1}$

Standard Free Energies of the Reactions Simulated in Figure 2B,C[b]		
reaction	calcd $\Delta G°$ (kcal/mol)	fitted $\Delta G°$ (kcal/mol)
$T1 + D1 \underset{k_{r1}}{\overset{k_{f1}}{\rightleftharpoons}} I$	−12.2	−9.00
$T2 + D1 \underset{k_{r2}}{\overset{k_{f2}}{\rightleftharpoons}} J$	−11.6	−8.95
$T2 + I \xrightarrow{k_{r2}} P1 + H1$	−6.8	N/A
$T1 + J \xrightarrow{k_{r1}} P1 + H1$	−7.4	N/A

[a] The simulations use the best-fit value of the rate constants; the errors bars on the rate constants are calculated as described in Materials and Methods, Parameter Fitting. [b] Calculated $\Delta G°$ (25 °C) denotes the value obtained from using the NUPACK predicted standard free energies of the complexes, and the fitted $\Delta G°$ denotes the value obtained from $\Delta G° = -RT\ln(k_f/k_r)$ The fitted $\Delta G°$ of the latter two reactions cannot be calculated because the reverse reaction was too slow to observe: according to the calculated $\Delta G°$, the reverse rate constant would be around 10 $M^{-1}\ s^{-1}$, corresponding to a time scale of about 3 months at an operational concentration of 10 nM.

Table 4. Reactions Simulated in Figure 3B,C[a]

reactions	rate constants
$T3 + D2 \underset{k_{r3}}{\overset{k_{f3}}{\rightleftharpoons}} I2$	$k_{f3} = 4 \times 10^6\ M^{-1}\ s^{-1}$
$T4 + D2 \underset{k_{r4}}{\overset{k_{f4}}{\rightleftharpoons}} J2$	$k_{f4} = 4 \times 10^6\ M^{-1}\ s^{-1}$
$T4 + I2 \xrightarrow{k_{f4}} P2 + H2$	$k_{r3} = 0.3\ s^{-1}$
$T3 + J2 \xrightarrow{k_{f4}} P2 + H2$	$k_{r4} = 0.2\ s^{-1}$

[a] The data displayed in Figure 3 underconstrain the rate constants. Shown here are one set of rate constant values that generated reasonably good agreement between ODE simulations and experimental data. Similar qualities of fit can be attained by co-varying the four rate constants.

different oligonucleotides, quantitation using cooperative hybridization may yield advantages over methods based on molecular beacons[47] because of the reduced need for calibration.

From the data shown in Figure 3B, the concentrations of *T*3 and *T*4 are implied to differ from their nominal values calculated from absorbance at 260 nm. Arbitrarily assuming that the concentration of *T*4 is accurate, the true concentration of *T*3 is inferred to be 14% lower than given. This 14% difference may arise due to errors in extinction coefficients, sample impurities that yield absorbance at 260 nm, and/or truncated oligonucleotides that cannot undergo cooperative hybridization. Figure 3C shows simulation results assuming that the concentrations of *T*3 are 14% lower than listed, and Figure 3D shows the equilibrium concentrations of *T*4 based on a variety of initial concentrations of *T*3 and *T*4 (with the corrected concentration of *T*3).

Table 4 shows the reactions simulated to generate the simulation traces shown in Figure 3C. Five different parameters were fitted to the data in Figure 3C (the four rate constants and the concentration of *T*3). Given the limited data on this system, the fit was underconstrained, and it is likely that many different sets of rate constant values would have yielded fits of similar quality.

The length of domain 6 is 7 nt, rather than 8 nt as in domains 1 and 4, because of the thermodynamically stabilizing effect of the 5′ dangle.[1] The length of domain 10 is 5 nt, rather than 7 or 8, because of the stabilizing effects of fluorophore−quencher binding on the thermodynamics of DNA hybridization.[48] Our own experiments suggest that the interaction between ROX and Iowa Black Red Quencher is similar to that of 4−5 base pairs binding (data not shown).

Reaction Networks Involving Cooperative Hybridization. Cooperative hybridization is a modular dynamic DNA nanotechnology component that can be integrated with other systems to form reaction networks with desired properties. In Figure 4, cooperative hybridization is cascaded with a DNA hybridization-based catalyst system[25] and a fluorescent reporter to yield a network that performs digital concentration comparison of two different oligonucleotides. This could potentially be used for detecting over-expression and under-expression of nucleic acids relative to certain thresholds.

In this reaction network, *T*2 serves as the catalyst for releasing *CP* from multistranded complex *CS*. Because *T*2 cooperatively hybridizes to *D*1 with *T*1, if the concentration of *T*1 exceeds that of *T*2, then little to no free *T*2 will exist, and *CP* will not be released. In contrast, if [*T*2] exceeds [*T*1], even if only by a little, then it catalytically releases *CP*, and the final fluorescence value will be determined by the concentration of precursor *CS* initially present in solution. Thus, the thresholded linear response shown in Figure 3C is converted to the sigmoidal thresholded response shown in Figure 4B,C. Alternative methods of digitally comparing nucleic acid concentrations using cooperative hybridization also exist (see Supporting Information, S5 and Figure S4).

In addition to providing a sigmoidal thresholded response, this reaction network also amplifies the fluorescence signal relative to the concentrations of the targets. In Figure 4B,C, the concentrations of *T*1 and *T*2 were both less than 10 nM, yet the final fluorescence corresponded to up to 20 nM of released fluorophore-labeled strands, demonstrating thresholded amplification using purely DNA components. Further amplification can be achieved through multilayer catalyst cascades or feedback systems.[25,49]

Logical Processing Using Cooperative Hybridization. The properties of cooperative hybridization can be interpreted as implementations of Boolean logic. For example, in Figure 1, *P*1 can be considered the output of a logical AND gate, with *T*1 and *T*2 being the inputs. Alternatively, in Figure 3, *T*4 can be considered the output of a logical NOT gate, with *T*3 being the input.

One key feature of Boolean logic is digital abstraction, wherein analog values are converted to digital ones through sigmoidal thresholding and amplification, both of which have been demonstrated in Figure 4. However, a simpler method of thresholding can be achieved using excess *L*1, the bottom strand of *D*1 (Figure 5A). Targets *T*1 and *T*2 preferentially bind *L*1 over *D*1 because *L*1 offers a longer single-stranded toehold for initiating hybridization and because individual hybridization is irreversible. Figure 5B shows that when either [*T*1] or [*T*2] is less than [*L*1], little product *P*1 is released; this is consistent with the assumption that *T*1 and *T*2 preferentially bind to *L*1.

Different cooperative hybridization elements can be cascaded with one another to exhibit more advanced logical functions. Here, the AND gate of Figure 1 is cascaded to the NOT gate of Figure 3 to form a reaction network exhibiting NAND logic (Figure 5C). Ordinarily, this would require one or more strand

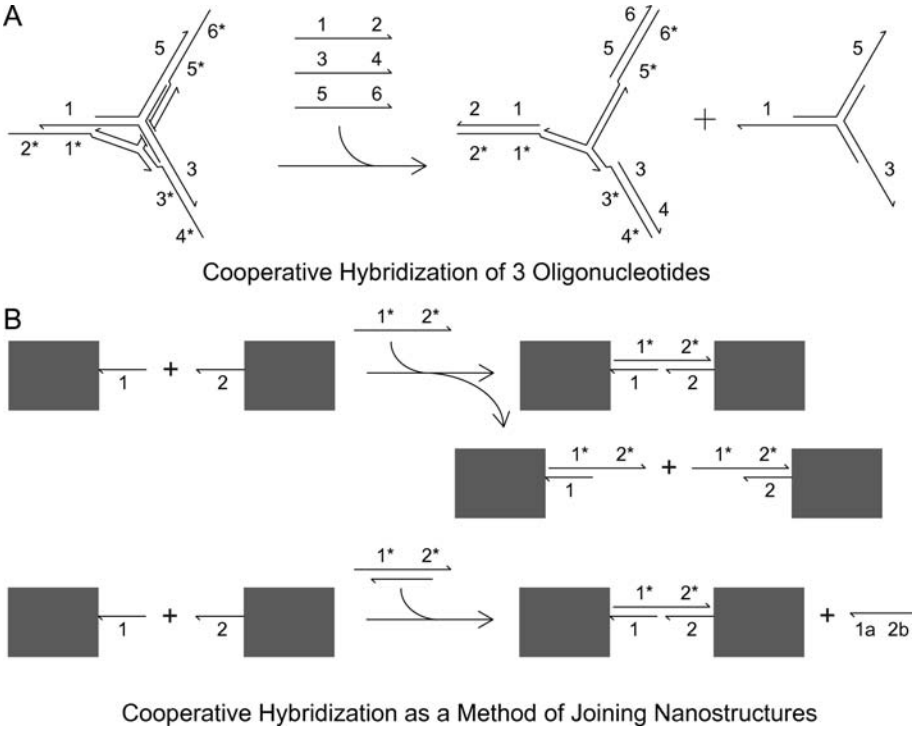

Figure 7. Potential extensions of cooperative hybridization. (A) Proposed method for extending cooperative hybridization to more than two targets. Note that the domain numbers present in this figure do not correspond to the domains shown in previous figures. Here, hybridization of even two targets to the device is reversible; only when all three targets bind does the top three-arm junction get released. (B) Proposed application of cooperative hybridization as a means of reliably joining DNA nanostructures. Joining DNA complexes or nanostructures using a complementary linker can cause unintentionally capping and prevent proper joining (top). In the cooperative hybridization mechanism (bottom), each overhang cannot individually hybridize stably to the linker, and joining can reliably occur.

displacement reactions to stoichiometrically convert *P*1 into *T*3.[23] However, in this case *T*3 was designed to be identical in sequence to *P*1, so that this stage can be eliminated. Figure 5D,E shows that the NAND network functions as designed: the observed fluorescence decreases only when both [*T*1] and [*T*2] exceed the threshold [*L*1].

Robustness. Thus far, all reactions have been tested in isolated solutions, in which no nucleic acids other than those needed were present. In order for the designed systems to function in either a biological setting or a complex synthetic chemical network, however, all designed reactions must be robust to a background of nucleic acids that interact nonspecifically.

Here, the robustness of cascaded cooperative hybridization reaction networks is tested by running the NAND reaction network in a solution of poly-N strands (Figure 6). The poly-N strands are each 50 nt long, with a random (G, C, A, T) base at every position with roughly equal probability. As $4^{50} > 10^{23}$, it is likely that every strand in the poly-N mix is different in sequence.

The reaction network functions qualitatively similarly, even in the presence of a 16× excess of poly-N over *T*1 and *T*2, attesting to the robustness and specificity of the cooperative hybridization mechanism. A standard hybridization assay is likely to be more disrupted by the presence of these poly-N strands, due to nonspecific binding interactions. Thus, the cooperative hybridization mechanism provides an additional degree of robustness and specificity over typical nucleic acid hybridization.

Extensions of Cooperative Hybridization. Cooperative hybridization is a general design principle for engineering nucleic acid devices and is by no means limited to those examples detailed in this manuscript. In this section, two extensions of the cooperative hybridization mechanism are proposed.

Cooperativity is a key feature of ensuring specific binding in both biological enzyme function and synthetic biotechnological devices. To construct devices that sense the simultaneous presence/colocalization of many oligonucleotides, increased cooperativity with Hill coefficient higher than 2 is desirable. One potential method of extending the cooperative hybridization mechanism introduced here is shown in Figure 7A. All three target oligonucleotides must be present to drive the hybridization reactions forward; any two of the three targets in isolation is insufficient and leads to only transient binding.

Similar methodology can be used to construct systems requiring four or more cooperative hybridization events. Alternatively, asymmetric branched DNA can also be used to implement three- and four-target cooperative hybridization. In cooperative hybridization of three or more oligonucleotides of independent sequence, geometry needs to be considered in addition to hybridization thermodynamics.

The controlled joining of DNA complexes or nanostructures could allow hierarchical, isothermal assembly of larger DNA nanostructures while preserving nanometer addressability. The use of linker oligonucleotides in a sandwich assay-like process, in which each subunit hybridizes irreversibly to the linker, can cause the subunits to be capped by the linker and preclude proper joining (Figure 7B). In the cooperative hybridization mechanism, each subunit individually cannot stably hybridize to the linker, so this problem is averted.

DISCUSSION

A cooperative nucleic acid hybridization mechanism was presented and verified in this work. In this mechanism, a two-stranded complex was designed so that two oligonucleotides of independent sequence can cooperatively and simultaneously hybridize to it. The cooperative hybridization mechanism is shown to be robust and modular, smoothly integrating with other dynamic DNA components to form cascaded reaction networks that perform a variety of functions.

The reactions shown here were rationally designed on the basis of the biophysics of nucleic acid hybridization, branch migration, and dissociation. Previous characterization of similar reactions has demonstrated that they function robustly across a wide range of solution salinities and temperatures,[25] as well as in the presence of total RNA and cell lysate.[23,25] Furthermore, similar strand displacement-based RNA devices have been made to assay and regulate gene expression in cells.[50−52] Thus, it is likely that many of these devices can be made to function *in situ* and *in vivo* for assaying and regulating gene expression.

Cooperative hybridization was demonstrated to implement analog subtraction and minimum functions. Both can serve important roles in the analysis and evaluation of biological nucleic acids, in which over- and under-expression of an RNA relative to a standard expression level can be indicative of disease. Integrating these elements with amplification and readout could potentially allow the construction of nucleic acid devices that perform embedded computation within cells, such as determining cell state from microRNA concentrations.

These analog primitives can also serve useful functions in the construction of synthetic circuits for controlling nanoscale self-assembly. In biology, cellular differentiation and development are often guided by the local relative expressions of different genes. Similarly, reaction−diffusion systems combining nucleic acid concentration gradients with concentration comparison circuits could lead to the formation of complex patterns and structures.

By combining cooperative hybridization with thresholding mechanisms, digital logic gates and circuits were constructed. Compared to previous implementations of nucleic acid logic gates and circuits based on strand displacement,[23,26] the major advantage of logic gates based on cooperative hybridization is the ease of sample preparation: the two-stranded complexes used for cooperative hybridization did not require any purification, either at the strand level or at the complex level. Furthermore, these systems are robust to nonspecific oligonucleotides coexisting in solution. These technical advantages reduces the labor needed to set up these circuits, thereby facilitating the construction of more complex reaction networks.

However, like previous implementations, the cooperative hybridization implementation of AND and NOT gates possesses certain limitations. Most notably, cooperative hybridization is a kinetically irreversible process, and logical values, once set, can never be reset. As a concrete example, in the NOT implementation (Figure 3), the *T*4 output strand binds irreversibly to *D*2 and *T*3, and so the output value of the NOT gate can only be changed from ON to OFF, and never from OFF to ON. This practically means that the NOT gate is not dynamic—it cannot, for example, be cascaded to form feedback circuits that require multiple value changes, such as a three-ring oscillator composed of three serially cascaded NOT gates in a feedback loop. Implementation of a dynamic nucleic acid-based logical NOT gate, in which the output concentration dynamically reflects changes in input concentrations, remains an open problem.

The cooperative hybridization mechanism enables more than just nucleic acid detection, quantitation, and logic; it is a fundamentally new design primitive that can allow simultaneity detection, precise timing control, nonlinear signal responses, and nanostructure joining. Integration of the cooperative hybridization mechanism with functional nucleic acids such as aptamers[53] and ribozymes,[54] expanded nucleic acid alphabets,[55] DNA-directed chemical synthesis,[56] or other nanomaterials[57] can broaden the set of chemistries that can serve as both input and output of an engineered nucleic acid system.

The complexity of natural biochemical circuits enables wondrous behaviors of life such as development, metabolism, and reproduction. It remains an outstanding goal of synthetic biology to rationally design reaction networks that exhibit similar spatial/temporal control of biochemistry; the design, demonstration, and integration of modular nucleic acid systems is one promising approach. The cooperative hybridization mechanism demonstrated in this paper may play an important role in constructing complex synthetic nucleic acid reaction and control networks.

ASSOCIATED CONTENT

Supporting Information. DNA sequence design, Matlab code for simulating reactions and fitting rate constants, characterization of individual rate constants, concentration quantitation from Figure 2, alternate mechanism for digitally comparing nucleic acid concentrations, and characterization of oligonucleotide purity using denaturing PAGE. This material is available free of charge via the Internet at http://pubs.acs.org.

AUTHOR INFORMATION

Corresponding Author
David.Zhang@wyss.harvard.edu

Present Addresses
[*]Wyss Institute, Harvard University, Boston, MA 02115.

ACKNOWLEDGMENT

The author thanks Erik Winfree and Georg Seelig for useful suggestions regarding the organization and presentation of the manuscript. The author is particular grateful to Erik Winfree for financial support for experimental reagents. This work was supported in part by NSF grants 0832824 and 0728703. D.Y.Z. was supported by the Fannie and John Hertz Foundation and is a Howard Hughes Medical Institute Fellow of the Life Sciences Research Foundation. There is a patent pending on the methods demonstrated in this paper.

REFERENCES

(1) SantaLucia, J.; Hicks, D. *Annu. Rev. Biochem.* **2004,** *33*, 415–440.
(2) Bloomfield, V. A.; Crothers, D. M.; Tinoco, I., Jr. *Nucleic Acids: Structures, Properties, and Functions*; University Science Books: Sausalito, CA, 2000.
(3) Carlson, R. *Nat. Biotechnol.* **2009,** *27*, 1091–1094.
(4) Aldaye, F. A.; Palmer, A. L.; Sleiman, H. F. *Science* **2008,** *321*, 1795–1799.
(5) Shih, W. M.; Lin, C. *Curr. Opin. Struct. Biol.* **2010,** *20*, 276–282.
(6) Lu, Y.; Liu, J. *Curr. Opin. Biotechnol.* **2006,** *17*, 580–588.
(7) Willner, I.; Shlyahovsky, B.; Zayats, M.; Willner, B. *Chem. Soc. Rev.* **2008,** *37*, 1153–1165.

(8) Bath, J.; Turberfield, A. J. *Nature Nanotechnol.* **2007,** *2,* 275–284.
(9) Zhang, D. Y.; Seelig, G. *Nature Chem.* **2010**, in press; DOI: 10.1038/NCHEM.957.
(10) Bartel, D. P. *Cell* **2009,** *136,* 215–233.
(11) Lu, J.; et al. *Nature* **2005,** *435,* 834–838.
(12) Rinker, S.; Ke, Y.; Liu, Y.; Chhabra, R.; Yan, H. *Nature Nanotechnol.* **2008,** *3,* 418–422.
(13) Maune, H. T.; Han, S.; Barish, R. D.; Bockrath, M.; Goddard, W. A.; Rothemund, P. W. K.; Winfree, E. *Nature Nanotechnol.* **2010,** *5,* 61–66.
(14) Winfree, E.; Liu, F.; Wenzler, L. A.; Seeman, N. C. *Nature* **1998,** *394,* 539–544.
(15) Rothemund, P. W. K.; Papadakis, N.; Winfree, E. *Plos Biol.* **2004,** *2,* 2041–2053.
(16) Rothemund, P. W. K. *Nature* **2006,** *440,* 297–302.
(17) Douglas, S. M.; Dietz, H.; Liedl, T.; Hogberg, B.; Graf, F.; Shih, W. M. *Nature* **2009,** *459,* 414–418.
(18) Zheng, J.; Birktoft, J. J.; Chen, Y.; Wang, T.; Sha, R.; Constantinou, P. E.; Ginell, S. L.; Mao, C.; Seeman, N. C. *Nature* **2009,** *461,* 74–77.
(19) Stojanovic, M. N.; Stefanovic, D. *Nat. Biotechnol.* **2003,** *21,* 1069–1074.
(20) Lederman, H.; Macdonald, J.; Stephanovic, D.; Stojanovic, M. N. *Biochemistry* **2006,** *45,* 1194–1199.
(21) Win, M. N.; Smolke, C. D. *Science* **2008,** *322,* 456–460.
(22) Levy, M.; Ellington, A. D. *Proc. Natl. Acad. Sci. U.S.A.* **2003,** *100,* 6416–6421.
(23) Seelig, G.; Soloveichik, D.; Zhang, D. Y.; Winfree, E. *Science* **2006,** *314,* 1585–1588.
(24) Seelig, G.; Yurke, B.; Winfree, E. *J. Am. Chem. Soc.* **2006,** *128,* 12211–12220.
(25) Zhang, D. Y.; Turberfield, A. J.; Yurke, B.; Winfree, E. *Science* **2007,** *318,* 1121–1125.
(26) Frezza, B. M.; Cockroft, S. L.; Ghadiri, M. R. *J. Am. Chem. Soc.* **2007,** *129,* 14875–14879.
(27) Zhang, D. Y.; Winfree, E. *J. Am. Chem. Soc.* **2008,** *130,* 13921–13926.
(28) Andersen, E. S.; et al. *Nature* **2009,** *459,* 73–76.
(29) Pei, R.; et al. *J. Am. Chem. Soc.* **2006,** *128,* 12693–12699.
(30) Lund, K.; et al. *Nature* **2010,** *465,* 206–210.
(31) Omabegho, T.; Sha, R.; Seeman, N. C. *Science* **2009,** *324,* 67–71.
(32) Green, S.; Bath, J.; Turberfield, A. J. *Phys. Rev. Lett.* **2008,** *101,* 238101.
(33) Yurke, B.; Turberfield, A. J.; Mills, A. P.; Simmel, F. C.; Neumann, J. L. *Nature* **2000,** *406,* 605–608.
(34) Yan, H.; Zhang, X. P.; Shen, Z. Y; Seeman, N. C. *Nature* **2002,** *415,* 62–65.
(35) Gu, H.; Chao., J.; Xiao, S.; Seeman, N. C. *Nature* **2010,** *465,* 202–205.
(36) Dirks, R. M.; Pierce, N. A. *Proc. Natl. Acad. Sci. U.S.A.* **2004,** *101,* 15275–1278.
(37) Venkataraman, S.; Dirks, R. M.; Rothemund, P. W. K.; Winfree, E.; Pierce, N. A. *Nature Nanotechnol.* **2007,** *2,* 490–494.
(38) Yin, P.; Choi, H. M. T.; Calvert, C. R.; Pierce, N. A. *Nature* **2008,** *451,* 318–322.
(39) Dirks, R. M.; Bois, J. S.; Schaeffer, J. M.; Winfree, E.; Pierce, N. A. *SIAM Rev.* **2007,** *49,* 65–88.
(40) Zhang, D. Y.; Winfree, E. *J. Am. Chem. Soc.* **2009,** *131,* 17303–17314.
(41) Yurke, B.; Mills, A. P. *Genet. Programming Evolvable Machines* **2003,** *4,* 111–122.
(42) Zhang, D. Y. *Lecture Notes Comput. Sci.* **2010**in press.
(43) Gao, Y.; Wolf, L. K.; Georgiadis, R. M. *Nucleic Acids Res.* **2006,** *34,* 3370–3377.
(44) Pyshnyi, D. V.; Ivanova, E. M. *Nucleosides, Nucleotides, Nucleic Acids* **2004,** *23,* 1057–1064.
(45) Puglisi, J. D.; Tinoco, I. *Methods Enzymol.* **1989,** *180,* 304–325.
(46) Owczarzy, R.; Moreira, B. G.; You, Y.; Behlke, M. A.; Walder, J. A. *Biochemistry* **2008,** *47,* 5336–5353.
(47) Tyagi, S.; Kramer, F. R. *Nat. Biotechnol.* **1996,** *14,* 303–308.
(48) Marras, S. A. E.; Kramer, F. R.; Tyagi, S. *Nucleic Acids Res.* **2002,** *30,* e122.
(49) Soloveichik, D.; Seelig, G.; Winfree, E. *Proc. Natl. Acad. Sci.U.S.A.* **2010,** *107,* 5393–5398.
(50) Seferos, D. S.; Giljohann, D. A.; Hill, H. D.; Prigodich, A. E.; Mirkin, C. A. *J. Am. Chem. Soc.* **2007,** *129,* 15477–15479.
(51) Isaacs, F. J.; Dwyer, D. J.; Ding, C. M.; Pervouchine, D. D.; Cantor, C. R.; Collins, J. J. *Nat. Biotechnol.* **2004,** *22,* 841–847.
(52) Venkataraman, S.; Dirks, R. M.; Ueda, C. T.; Pierce, N. *Proc. Natl. Acad. Sci. U.S.A.* **2010,** *107,* 16777–16783.
(53) Bunka, D. H. J.; Stockley, P. G. *Nat. Rev. Microbiol.* **2006,** *4,* 588–596.
(54) Joyce, G. F. *Annu. Rev. Biochem.* **2004,** *73,* 791–836.
(55) Krueger, A. T.; Kool, E. T. *Chem. Biol.* **2009,** *16,* 242–248.
(56) Gartner, Z. J.; Tse, B. N.; Grubina, R.; Doyon, J. B.; Snyder, T. M; Liu, D. R. *Science* **2004,** *305,* 1601–1605.
(57) Rosi, N. L.; Mirkin, C. A. *Chem. Rev.* **2005,** *105,* 1547.